fermentation

MDPI

Article

Improvement of Biohydrogen and Usable Chemical Products from Glycerol by Co-Culture of *Enterobacter* spH1 and *Citrobacter freundii* H3 Using Different Supports as Surface Immobilization

Biniam T. Maru [1,2], Francisco Lopez [1], Francesc Medina [1] and Magda Constantí [1,*]

[1] Departament d'Enginyeria Química, Universitat Rovira i Virgili, Av. Països Catalans, 26, 43007 Tarragona, Spain; Bmaru@whitedoglabs.com (B.T.M.); francisco.lopez@urv.cat (F.L.); francesc.medina@urv.cat (F.M.)

[2] White Dog Labs Inc., 239 Lisa Drive, New Castle, DE 19720, USA

* Correspondence: magda.constanti@urv.cat

Abstract: Glycerol is a by-product of biodiesel production in a yield of about 10% (*w*/*w*). The present study aims to improve the dark fermentation of glycerol by surface immobilization of microorganisms on supports. Four different supports were used—maghemite (Fe_2O_3), activated carbon (AC), silica gel (SiO_2), and alumina (γ-Al_2O_3)—on which a newly isolated co-culture of *Enterobacter* spH1 and *Citrobacter freundii*, H3, was immobilized. The effect of iron species on dark fermentation was also studied by impregnation on AC and SiO_2. The fermentative metabolites were mainly ethanol, 1,3-propanediol, lactate, H_2 and CO_2. The production rate ($R_{max,i}$) and product yield (Yi) were elucidated by modeling using the Gompertz equation for the batch dark fermentation kinetics (maximum product formation ($P_{max,i}$): (i) For each of the supports, H_2 production (mmol/L) and yield (mol H_2/mol glycerol consumed) increased in the following order: FC < γ-Al_2O_3 < Fe_2O_3 < SiO_2 < Fe/SiO_2 < AC < Fe/AC. (ii) Ethanol production (mmol/L) increased in the following order: FC < Fe_2O_3 < γ-Al_2O_3 < SiO_2 < Fe/SiO_2 < Fe/AC < AC, and yield (mol EtOH/mol glycerol consumed) increased in the following order: FC < Fe_2O_3 < Fe/AC < Fe/SiO_2 < SiO_2 < AC < γ-Al_2O_3. (iii) 1,3-propanediol production (mmol/L) and yield (mol 1,3PDO/mol glycerol consumed) increased in the following order: γ-Al_2O_3 < SiO_2 < Fe/SiO_2 < AC < Fe_2O_3 < Fe/AC < FC. (iv) Lactate production(mmol/L) and yield (mol Lactate/mol glycerol consumed) increased in the following order: γ-Al_2O_3 < SiO_2 < AC < Fe/SiO_2 < Fe/AC < Fe_2O_3 < FC. The study shows that in all cases, glycerol conversion was higher when the support assisted culture was used. It is noted that glycerol conversion and H_2 production were dependent on the specific surface area of the support. H_2 production clearly increased with the Fe_2O_3, Al_2O_3, SiO_2 and AC supports. H_2 production on the iron-impregnated AC and SiO_2 supports was higher than on the corresponding bare supports. These results indicate that the support enhances the productivity of H_2, perhaps because of specific surface area attachment, biofilm formation of the microorganisms and activation of the hydrogenase enzyme by iron species.

Keywords: glycerol; biohydrogen; support; *Enterobacter*; *Citrobacter freundii*; maghemite; activated carbon; silica gel; alumina

Citation: Maru, B.T.; Lopez, F.; Medina, F.; Constantí, M. Improvement of Biohydrogen and Usable Chemical Products from Glycerol by Co-Culture of *Enterobacter* spH1 and *Citrobacter freundii* H3 Using Different Supports as Surface Immobilization. *Fermentation* **2021**, *7*, 154. https://doi.org/10.3390/fermentation7030154

Academic Editor: Diomi Mamma

Received: 23 June 2021
Accepted: 12 August 2021
Published: 15 August 2021

1. Introduction

Hydrogen is now accepted as an attractive, clean, and renewable energy carrier. It is an important area of bioenergy production and bioremediation [1,2]. At present, most H_2 is generated by thermochemical processes that use fossil fuels such as natural gas, thermal cracking and coal gasification [1]. However, these processes emit CO_2.

Lately, a considerable amount of attention has been paid to biological processes such as biophotosynthesis, photodecomposition and anaerobic fermentation routes to harmless H_2 from renewable sources such as water, waste organic matter and organic compounds [3,4].

Of all these processes, dark fermentation seems to be the best, because it is not only the most stable but also the most rapid. Additionally, unlike photofermentation, it can be carried out in the absence of light [1,5]. It also uses obligate and facultative anaerobic microorganisms to convert organic materials into H_2 from the general anaerobic metabolism.

Dark fermentation can use various organic wastes as substrates for biohydrogen production. Glycerol is an attractive, cheap resource, as it is a by-product of biodiesel production with a yield of about 10% (wt/wt). In addition to being widely available [6] and economic, it also has the potential to mitigate environmental hazards and reduce greenhouse gas (GHG) emissions. The main advantage of using glycerol in dark fermentation is the production of fuels and chemical products at a higher yield than the common sugars such as glucose and xylose, due to the high redox state of the carbon in the glycerol [7]. Henceforth, the production of H_2 through dark fermentation is an alternative for conventional fossil fuels. However, it has one major drawback: a low yield of hydrogen production [1]. In order to improve the performance of dark fermentation using glycerol, new biological activities such as support immobilization can be used as one strategy to enhance the yield of hydrogen production.

Cell immobilization technology has been used in fermentation and enzymatic transformation [8]. Gungormusler et al. [9] showed that entrapped cells of the *Clostridium intestinale* strain URNW produced more hydrogen than suspended cultures, and Chen [10] found that carrier supports were effective at stimulating cell growth and the production of targeted metabolites. Likewise, the immobilization of *Enterobacter aerogenes* on carbon fiber and activated carbon enhanced both the hydrogen production rate and hydrogen yield [11]. In previous work, Lee et al. [12] showed that the addition of an appropriate amount of solid carrier, such as activated carbon, to the fermentation broth could markedly stimulate cell growth and H_2 production in dark fermentation. Other reports also showed that solid carriers were effective at stimulating cell growth and target metabolite production of, for example, H_2 and biosurfactants [13–16]. Carriers are thought to provide more surface attachment sites, which enhance the formation of biofilms [17] and granular sludge [14,18]. Solid carriers can also provide buffer capacity for extreme conditions such as high organic loadings, pH shock, etc. [17,18]. Like immobilized cells, carriers can enhance cell retention for continuous cultures, thereby preventing cell wash-out while operating at a high dilution rate (or a low hydraulic retention time) [19,20]. On the other hand, the type and concentration of the carbon substrate are critical factors that affect the fermentation kinetics of biohydrogen production [21]. The structure and morphology of the micro-beads have a considerable influence on physical properties and, therefore, on the reactivity of the functional sites [22].

The glycerol bioconversion pathways to H_2 are based on a simple redox reaction: $2H^+ + 2e^- \leftrightarrow H_2$ [23]. This reaction is catalyzed by hydrogen-producing enzymes, namely [NiFe]-hydrogenases and [FeFe]-hydrogenases, which are mostly present in anaerobic bacteria [23–27]. This process takes place after glycerol enters the glycolysis pathways to produce pyruvate. Pyruvate then breaks down to acetyl-CoA via reduction of a ferredoxin (Fd) catalyzed by pyruvate ferredoxin oxidoreductase [28,29]. The hydrogenase enzyme (E.C.1.12.7.1) then oxidizes the reduced ferredoxin (Fd) to produce molecular hydrogen [24].

Hydrogenase enzymes are clusters of FeFe or NiFe. Therefore, it is to be assumed that iron species can affect their activity. Some studies have reported that the in vivo activity of the hydrogenase decreases with iron depletion [29,30] and that hydrogen production improves with iron addition [31,32]. However, these studies mainly focused on biochemical production with glucose as a substrate and little work has been done on H_2 production with glycerol as a substrate. In addition, surface attachment immobilization techniques have not been widely adapted to H_2 production through dark fermentation from glycerol [33]. Hence, a study is needed in this field to evaluate the yield of hydrogen from glycerol by immobilizing iron species on the surface. Our previous study showed that *Enterobacter* spH1 and *Citrobacter freundii* metabolize glycerol to hydrogen [34]. However, the hydrogen rate production and glycerol conversion were low; therefore, in this study, we intend to

increase the rate of H_2 production and increase glycerol consumption by incorporating support to the cells.

In this paper we also aimed to assess the effectiveness and feasibility of the surface cell immobilization of a co-culture (1:1) of *Enterobacter* and *Citrobacter* sp on four different porous solid supports: maghemite (Fe_2O_3), activated carbon (AC), silica gel (SiO_2) and alumina (γ-Al_2O_3) via batch dark fermentation. These supports are selected because they have been proven to provide good surface area attachment sites in catalytic processes and cell immobilization [35,36]. Some previous studies also show these kinds of supports will stimulate cell growth and hydrogen production, provide buffer capacity, and enhance cell retention times. The effect of iron species on the dark fermentation for H_2 production was also investigated on AC and SiO_2.

2. Materials and Methods

2.1. Fermentable Substrates and Chemicals

Pure glycerol (molecular biology, purity $\geq$ 99%) and all other chemicals of analytical grade were purchased from Sigma Chemical Co., Madrid, Spain. Support materials were supplied by Merck, Madrid, Spain: activated carbon ref. 2518 and silica gel ref. 2518.

2.2. Microorganism, Medium and Culture Conditions

2.2.1. Microorganisms

Enterobacter spH1 and *Citrobacter freundii* H3 (isolated from San Carles de la Rapita, Spain), which are known to be able to produce H_2 from glycerol, were used as a co-culture [34]. Standard microbiological and safety procedures were followed while the cultures were being handled.

2.2.2. Culture Medium

The mixed (1:1) co-culture was cultivated in synthetic medium consisting of (amounts are in grams per liter of deionized water): 7.0 g K_2HPO_4; 5.5 g KH_2PO_4; 1.0 g of $(NH_4)_2SO_4$; 0.021 g of $CaCl_2 \cdot 2H_2O$; 0.25 g of $MgSO_4 \cdot 7H_2O$; 0.25 g of $MgSO_4 \cdot 7H_2O$; 0.021 g of $CaCl_2 \cdot 2H_2O$; 0.12 g of $Na_2MoO_4 \cdot 2H_2O$; 2.0 mg of nicotinic acid, 0.172 mg of Na_2SeO_3, 11.9 g HEPES (N-2-hydroxyethylpiperazine-N-2 ethanesulphonic acid); 0.5 g of yeast extract (YE); 10 mL of trace element solution containing 0.5 g of $MnCl_2 \cdot 4H_2O$, 0.1 g of H_3BO_4, 0.01 g of $AlK(SO_4)_2 \cdot H_2O$, 0.001 g of $CuCl_2 \cdot 2H_2O$ and 0.5 g of Na_2EDTA per liter; 0.5 g/L of cysteine hydrochloride as reducing agent and 1 mg resazurin, which was used as a redox indicator. Anaerobic conditions were achieved by flushing the headspace of the serum bottles with Ar gas before inoculating for about 3–4 h until the resazurin changed to colorless. Additionally, before inoculating, the medium pH was adjusted to 6.5 for each strain using 10 mM NaOH.The medium used was appropriate for H_2 production since it contained the minimum nutrients required [37].

2.2.3. Support Materials

The mixed co-culture of *Enterobacter* spH1 and *Citrobacter freundii* H3 was used to examine the effect of support on the dark fermentation of glycerol to produce H_2. Four different supports were used: maghemite (Fe_2O_3), activated carbon (AC), silica gel (SiO_2) and alumina (γ-Al_2O_3). The effect of impregnating iron species on AC and SiO_2 on the dark fermentation was also studied. Iron supported on AC was prepared by incipient wetness impregnation with aqueous solution and ferrous sulphate ($FeSO_4 \cdot 7H_2O$) as a precursor. The iron load was 10 wt%. After impregnation, the solids were left for 2 h at room temperature (RT), dried for 15 h at 60 °C and finally calcinated at 200 °C for 4 h [38]. Before use, each support was washed with distilled H_2O to remove all suspended fine colloidal particles and then autoclaved for 20 min at 121 °C to eliminate microbial contaminants.

2.3. Batch Dark Fermentation

Batch cultivations were performed in 100 mL serum bottles fitted with gas-tight crimp-top rubber septa and flushed with Ar for 15 min. They had a working volume of 25 mL, were kept at a constant temperature of 37 °C and were shaken at 200 rpm. Cultures were inoculated with 10% (*v*/*v*) pre-culture. The effect of the six different assisted carriers (2% (*w*/*v*)) on the fermentation was tested for mixed culture. A control batch experiment was done for each support (2% (*w*/*v*)) without culture to measure the adsorption capacity (Q) of each support. The control and main experiment were prepared with the same synthetic medium containing 25 g/L glycerol.

2.4. Analytical Methods

2.4.1. Biomass Growth

For the carrier-assisted batch dark fermentation, the biomass growth was determined using the sum of the cells which grow freely in the liquid culture and the cells attached to the support. An 0.8 mm filter was used to separate the attached cells from the freely suspended ones. Samples for analysis were taken at the beginning and at the end of fermentation.

The residue on the filter was washed with 10 mL deionized water and centrifuged (600× *g*, 15 min at 4 °C), and the supernatant was discarded. The cells attached to the support remained as a residue on the filter and were then re-suspended in 2 mL ultrapure water and dried for SEM and N_2 physisorption analysis. A total of 1 mg of this residue (containing attached cells and the support) was used for scanning electron microscopy (SEM) morphological studies. The number of cells attached to the support carrier were estimated per m^2 by direct cell counting from the SEM pictures using ImageJ 1.46 r software. The total of the attached cells was obtained by multiplying by the cells counted per m^2 of the support.

Cell growth was determined using an optical density at 600 nm (OD_{600}). After filtering, the optical density (OD) of the filtrate was measured at 600 nm, which corresponds to the unattached cells. Additionally, cell dry weight (CDW) was used to quantify the amount of biomass in the serum bottle. CDWs were determined in technical duplicates. 2 × 15 mL cultures were sampled and centrifuged (600× *g*, 15 min at 4 °C). Each pellet was resuspended in 2 mL ultrapure water. CDWs were determined after the samples had been dried for 1 day in an oven at 105 °C. OD_{600} and CDW were then correlated using CDW = 857.716 × OD, with R^2 = 0.8782.

2.4.2. Analysis of Gas Production

During batch experiments, the H_2 and CO_2 in the serum bottle headspaces were quantified by GC-14B GC, with a thermal conductivity detector (TCD) and a Carbosive column and a 80/100 Porapak-Q column (Merck, Madrid, Spain) with argon (Ar) and helium (He) as carrier gas and a flow rate of 30 mL/min. The operational temperatures for the injection port, oven and detector were 150, 80 and 200 °C, respectively.

A gastight syringe was used to sample the gas produced from the processed anaerobic bottle. The syringe has a valve that can be closed to trap the gas inside. A total of 0.3 mL of gas was taken and equilibrated at atmospheric pressure. The system was calibrated using an H_2 standard to determine the volume of gas as a percentage. The H_2 gas was identified by using GC equipped with a thermal conductivity detector (TCD). The peak corresponds to a certain volume percent of H_2. The volume fraction of H_2 in the syringe was equivalent to the volume fraction of H_2 in the headspace when the gas from the processed serum bottle was sampled. The total volume of H_2 was calculated by multiplying the volume percentage by the headspace of the serum bottle, so the ideal gas law can be used to calculate the number of moles of gas produced.

2.4.3. Analysis of Liquid Metabolites

Fermentation products were identified by HPLC, using a Transgenomic column, (ICSep ICE-COREGEL 87H3, Chrom Tech, MN, USA) equipped with diode array (DAD) and refractive index (RID) detectors. Aqueous sulfuric acid (H_2SO_4) adjusted to pH 2.2 was used as the mobile phase. Operating conditions for the HPLC column were 50 °C with a mobile phase flow rate of 0.6 mL/min. Prior to analysis, the liquid samples were centrifuged at 9800 rpm for 15 min and filtered through a 0.2 µm disposable filter. The injection volume of the sample was 20 µL. The sample eluted completely within 40 min. Concentrations of fermentation metabolites were determined using standard curves of the respective compounds.

GC-MS was equipped with an HP PLOT column (divinylbenzene/styrene polymer, 30 m long, 0.32 mm ID, 20 µm film thickness, Agilent, CA, USA) and operated at an inlet temperature of 200 °C, a pressure of 6.1 psi and an oven temperature of 35 °C for 5 min increasing to 150 °C at 5 °C/min. Prior to the CG-MS analysis, the liquid samples were centrifuged at 9800 rpm for 15 min and filtered through a 0.2 µm disposable filter. The injection volume of the sample was 5 µL. Glycerol and product fermentation metabolites in the liquid phase were confirmed by GC-MS.

2.4.4. Support Characterization

The morphology of the mixed culture cells attached to each carrier was examined by scanning electron microscopy (SEM, JEOL JSM-840, Tokyo, Japan) at 20 kV and a working distance of 15 mm. Prior to SEM observation, samples were fixed with 2% *w*/*w* glutaraldehyde and dehydrated in graded series of ethanol. Finally, the samples were dried with a critical point dryer (EMS-850, Tokyo, Japan) coated with gold [39].

N_2 physisorption adsorption–desorption isotherms at 77 K were measured using Micromeritics ASAP 2000 (GA, USA) equipment for the analysis of specific surface area (S_{BET}), average pore volume and pore size. Prior to the physisorption measurements, all the samples were degassed under vacuum (10^{-4} Pa) at 393 K. N_2 physisorption was used to reveal information about the texture properties of each carrier before and after the batch fermentation.

X-ray diffraction (XRD) analysis was used to determine any changes on the surface of the carrier before and after fermentation. The XRD analysis of the carrier was recorded using a Siemens D5000 diffractometer (Rubí, Spain) (Bragg–Brentano geometry and vertical θ-θ goniometer) with an angular 2θ diffraction range between 3° and 90°. The samples were placed on a Si (510) sample holder. The data were collected with an angular step of 0.03° at 5 s per step and sample rotation. Cu Kα radiation (λ = 1.54056 Å) was obtained from a copper X-ray tube operated at 40 kV and 30 mA. The crystalline phases were identified using JCPDS powder diffraction files as data references.

2.4.5. Total Organic Carbon Analysis

The concentration of total organic carbon (TOC) before and after batch fermentation was measured using a Total Organic Carbon Analyzer (Analytik jena, Multi N/C 2100, Jena, Germany). Prior to analysis the liquid sample was filtered through a 0.2 µm disposable filter.

2.5. Data Analysis

Data Analysis and Kinetic Parameters

The adsorption capacity of the adsorbents (support) was calculated from the change in glycerol concentration in the solution using Equation (1), where *Q* is the adsorption capacity (mg/g), *Ms* is the amount of adsorbent, $Q_{Gly\ cons,f}$ is glycerol consumed by microbes and *QGly,i* and *QGly,f* are the glycerol concentrations before and after fermentation, respectively As mentioned above, glycerol concentration was determined by HPLC.

$$Q = \frac{(\ Q_{Gly,i} - Q_{Gly,f}) + \left(\ Q_{Gly\ cons,\ f}\right)}{M_s} \quad (1)$$

A modified Gompertz equation Equation (2) [40,41] was used to estimate the maximum production rates and the maximum production potentials of such fermentation end products as: ethanol, acetate, lactate, propionate, succinate, 2, 3 butanediol, CO_2 and H_2:

$$S_0 - S(t) = S_{\max}.\exp\left\{-\exp\left[\frac{R_{\max,S}\ .e}{S_{\max}}(\lambda_S - t) + 1\right]\right\} \quad (2)$$

where $P_i(t)$ is the cumulative production (mmol/L), λ the lag-phase time (h), $P_{max,i}$ the maximum production potential (mmol/L), $R_{max,i}$ the maximum production rate (mmol/L*h), t the incubation time (h), and e the $exp(1)$ = 2.718. This equation was found to be suitable for describing the progress of the cumulative production of compounds during the experiments.

Accordingly, for the consumption of glycerol a modified Gompertz equation Equation (3) [40] was used:

$$S_0 - S(t) = S_{max}exp\left\{-exp\left[\frac{R_{max,S}\ e}{S_{max}}(\lambda_S - t) + 1\right]\right\} \quad (3)$$

where: S_0 is initial substrate concentration (mmol/L), S is substrate concentration (mmol/L) at time t, S_{max} is maximum concentration of consumed substrate (mmol/L) and $R_{max,S}$ is maximum rate of substrate consumption (mmol/L×h). The fermentation data was fitted using SigmaPlot version 12.3, CA, USA,where the accuracy of fit was given by correlation coefficients (R^2).

For batch cultivation yields of the fermentation end-products, expressed in mole product per mole of glycerol consumed, the experimental data of the substrate adsorbed in Equation (1) was considered in the yield calculation (Equation (4)).

$$Y_{P\ max,\ i} = \frac{P_{max,\ i}}{S_0 - (S_{max} - S_{ads})} \quad (4)$$

where: $Y_{Pmax,i}$ is substrate yield for fermentation product i, S_0 is initial glycerol concentration (mol/L), S_{max} is maximum glycerol consumption (mol/L) and S_{ads} is maximum glycerol adsorbed by the support (mmol/L).

Maximum specific production or consumption ($q_{max,i}$) were calculated using the values obtained from the data fits (Equations (2) and (3)), according to Equations (5) and (6) respectively, and the ratio of the maximum production rate or substrate consumption rate to the maximum dry cell weight (DCW_{max}).

$$q_{max,i} = \frac{R_{max,i}}{DCW_{max}} \quad (5)$$

$$q_{max,s} = \frac{S_{max,i}}{DCW_{max}} \quad (6)$$

where: $q_{max,i}$ is the specific production or consumption rate i (mmol/L*h), $R_{max,i}$ is the maximum production rate i, $S_{max,i}$ is the maximum substrate consumption rate (mmol/L*h) and DCW_{max} is the maximum dry cell weight (g/L).

Carbon balances (C-balance) and degree of reduction balances (ε-balance) were calculated according to Oh et al. and Converti et al. using the elemental biomass composition $CH_{1.74}O_{0.33}N_{0.23}$ [34,37]. This corresponds to a biomass carbon content of 53.6% and a degree of reduction of 4.32 electrons per C atom. The degree of reduction (ε) was calculated from the following Equation (7) [42,43].

$$\varepsilon = 4C + H - 2O - 3N \quad (7)$$

where *C*, *H*, *O*, and *N* denote the atomic coefficient of the chemical formula of a compound.

Glycerol conversion (*E*) by the strains was calculated using the following equation Equation (8):

$$E = \frac{S_0 - (S_{max} - S_{ads})}{S_0} \times 100 \quad (8)$$

Determining hydrogen and CO_2 production. The number of moles of gas (*n*) injected into GC at room temperature was calculated using the ideal gas law in Equation (9).

$$PV = nRT \quad (9)$$

where *P* is atmospheric pressure, *V* is the volume determined by the injection, *R* is universal gas constant and *T* is *RT*.

3. Results and Discussion

3.1. Textural Characteristics of Supports

The textural characteristics of each support used for dark fermentation are summarized in Table 1. The N_2 physisorption of the carrier was performed before and after the dark fermentation.

Table 1. Textural properties of the *Enterobacter* spH1 and *Citrobacter freundii* H3 co-culture supports used in the dark fermentation.

Carrier	Before Dark Fermentation			After Dark Fermentation		
	* S_{BET} (m^2/g)	Porous Volume (cm^3/g)	Porous Size (nm)	S_{BET} (m^2/g)	Porous Volume (cm^3/g)	Porous Size (nm)
Fe_2O_3	205	0.779	13.99	158	0.403	2.897
γ-Al_2O_3	253	0.450	4.54	105	0.192	2.271
SiO_2	685	0.822	3.32	202	0.347	1.872
Fe/SiO_2	440	0.540	2.84	150	0.251	1.871
AC	1195	0.675	1.69	462	0.269	1.614
Fe/AC	736	0.413	0.84	382	0.085	0.807

* S_{BET} stands for specific surface area Brunauer–Emmett–Teller measured in nitrogen adsorption.

Table 1 shows the surface area, pore volume and pore size for the different carriers before and after the dark fermentation. The addition of iron species to the SiO_2 and AC carriers decreased the surface area and pore volumes for both supports, which suggests that impregnation with iron species presumably blocks the carrier pores. Maghemite (Fe_2O_3), silica gel (SiO_2) and alumina (γ-Al_2O_3) exhibited the typical mesoporous type IV isotherms (Figure 1a–c) according to the Brunauer–Deming–Deming–Teller (BDDT) classification. Activated carbon (AC) (Figure 1d) exhibited a microporous structure with type I isotherms characterized by a plateau that is nearly horizontal to the $P/P_\circ$ axis.

After dark fermentation the total surface area, pore volume, and porous size of all materials decreased presumably because of the growth of the microorganisms and the adsorption of organic metabolites.

Several studies that have used AC as the catalyst reveal a significant modification in both the texture and surface group distribution of the original AC in the course of the experiment [44].

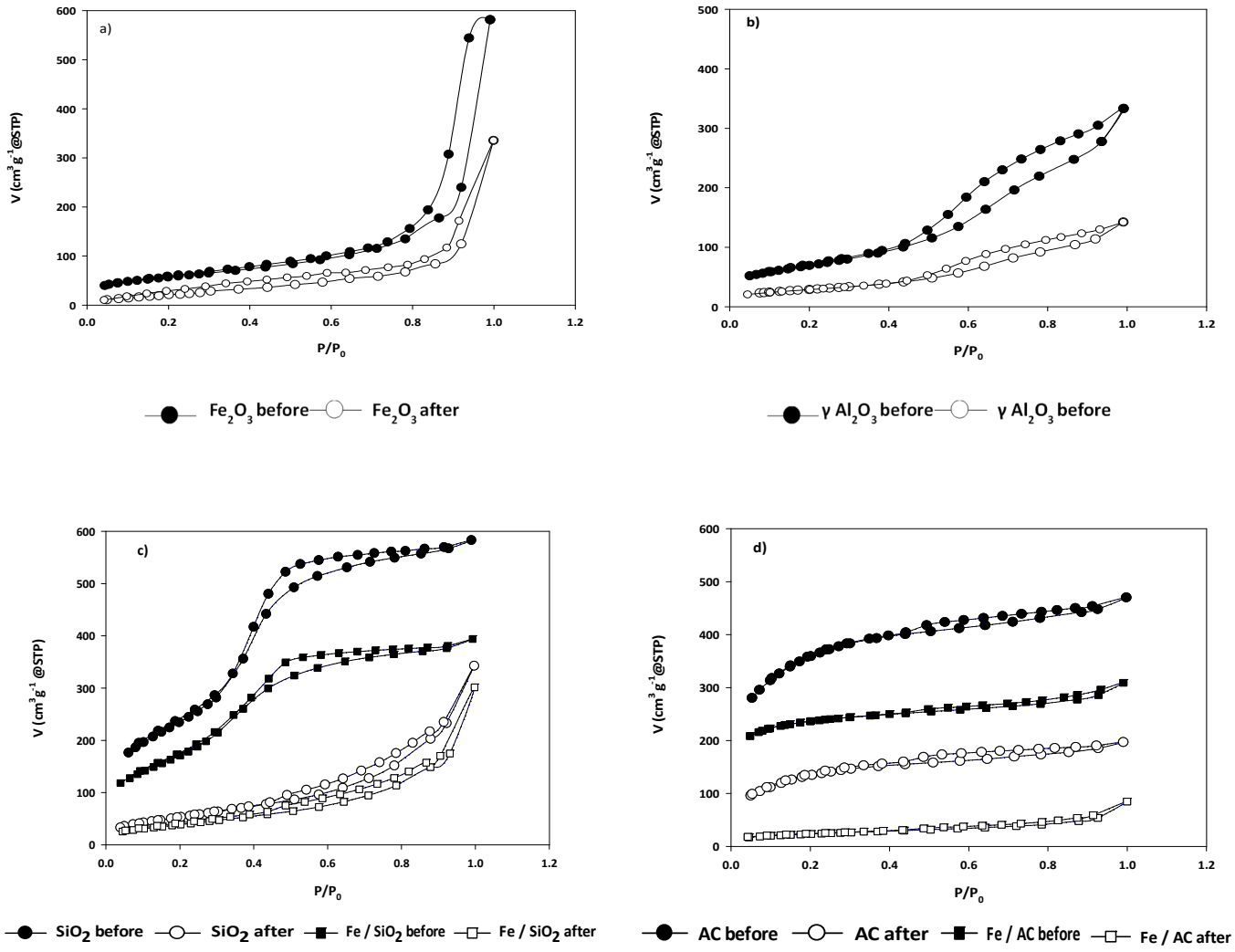

Figure 1. N_2 adsorption–desorption isotherms for support before and after the batch dark fermentation: (**a**) Fe_2O_3; (**b**) γ-Al_2O_3; (**c**) SiO_2 and Fe/SiO_2; (**d**) AC and Fe/AC.

3.2. Support Characterization

As can be observed in Figure 2a, no other species other than carbon is observed for activated carbon before the fermentation. This XRD pattern shows that only the graphite phase is present in the activated carbon. This indicates the purity of the activated carbon used in the experiment, and this will help compare the AC after the experiment depicted in Figure 2b.

After the dark fermentation, the XRD profile of the activated carbon support (Figure 2b) shows the crystallographic phases of the Ramsbeckite (JCDPS 39-0365). This copper species probably comes from the adsorption of metal species such as copper in the culture medium.

The XRD profile of all the supports (Figure 2c) after the dark fermentation also shows the crystallographic phases of the Ramsbeckite (JCDPS 39-0365). This copper species probably comes from the adsorption of metal species such as copper in the culture medium.

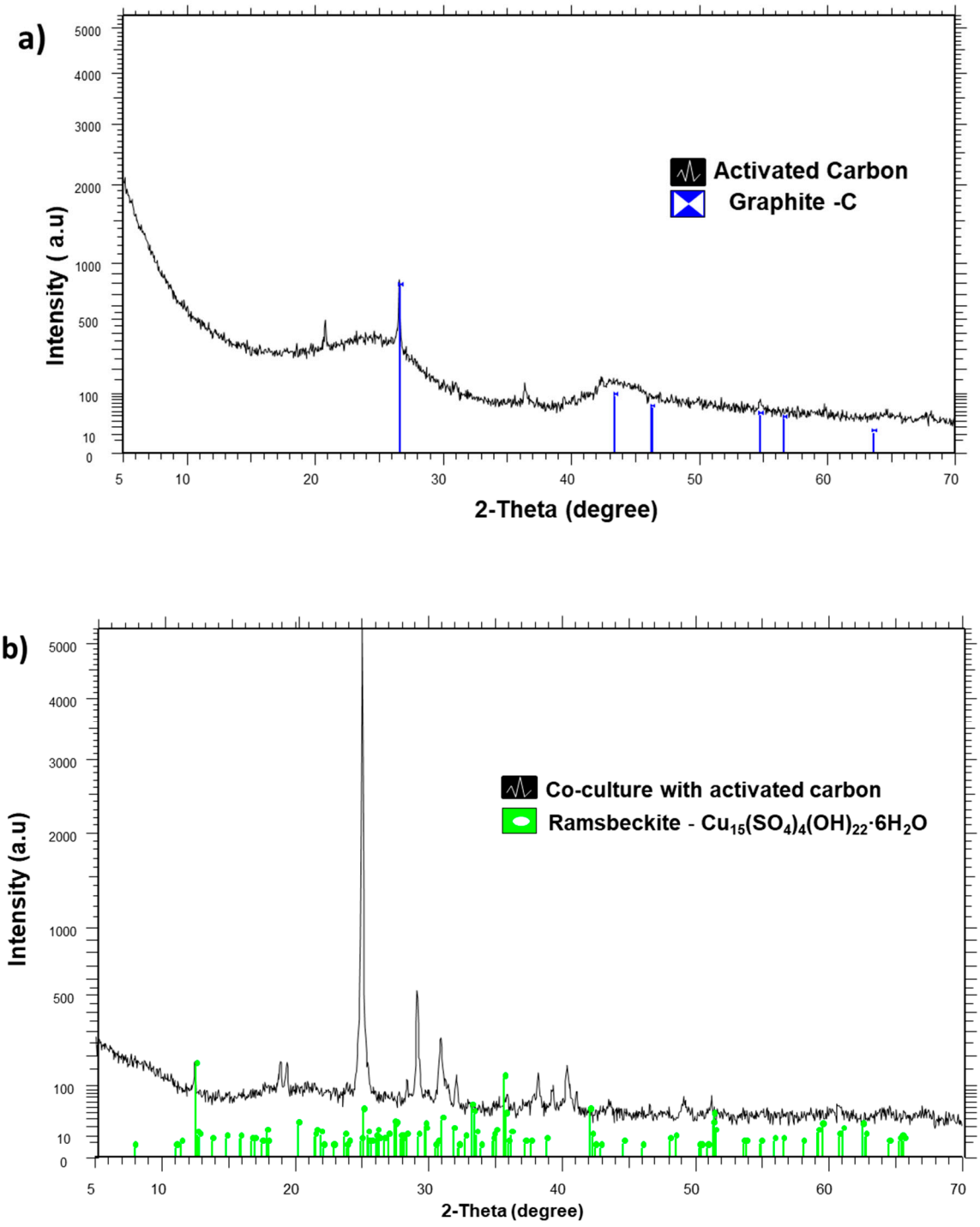

Figure 2. *Cont.*

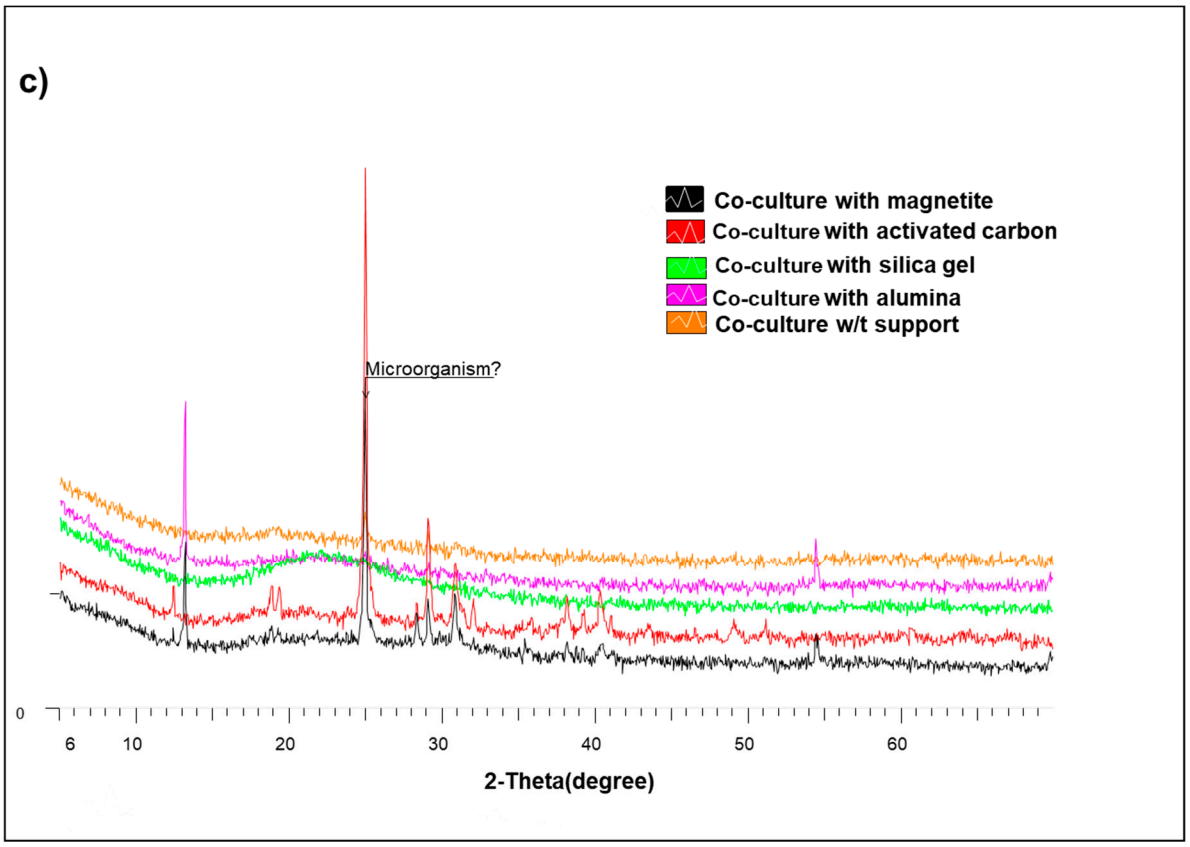

Figure 2. Powder XRD patterns: (**a**) AC before dark fermentation; (**b**) AC after dark fermentation; and (**c**) all supports after dark fermentation.

3.3. Morphology and Count of Cells Attached to the Support

The surfaces of the immobilized cells were studied by scanning electron microscopy (SEM). The number of bacteria attached was counted using ImageJ 1.46 r software, MD, USA. Figure 3 shows the random distribution of cells on each support. The number of attached bacteria is higher after fermentation; however, alumina shows the lowest density. The support surfaces look different showing distinct images of bacterial attachments.

Effect of Supports on Bacterial Surface Attachment

As can be observed, Figure 4 presents the attached cell counts of mixed cultures. It shows that the cell population improves in the following order: AC > SiO_2 > Fe/AC ≥ Fe/SiO_2 > γ-Al_2O_3 > Fe_2O_3. This might be due to the surface area and roughness. There was a qualitative increase in the number of attached cells on the AC than the other supports. Attached cells or biofilms are defined as matrix-enclosed bacterial populations, which adhere to each other and the support surfaces [45]. Biofilm-attached bacteria predominate numerically and metabolically in virtually all ecosystems [46]. Costerton et al. [43] reported that the substratum structure promotes the attachment of bacteria to the surface, and there is considerable evidence that attachment increases with increasing surface roughness or rugosity of the support. Other factors, such as the coating of the substratum with biomolecules, e.g., proteins and polysaccharides, and the hydrodynamic flow velocity immediately adjacent to the substratum, also influence biofilm formation. In addition, cellular properties of bacteria such as the presence of fimbriae and flagella, and the production of extracellular polymers increase bacteria attachment [47,48]. Indeed, the sugar analysis of exopolysacharides isolated from *Citrobacter freundii* showed the presence of mannose and glucose [49]. The concentrations of nutrients in the aqueous medium surrounding the attached cell also affect biofilm development.

Previous laboratory studies indicate that there is a correlation between an increase in nutrient concentrations and increased numbers of attached bacterial cells [50]. Indeed, it has also been speculated that surface associations offer selective growth advantages for attached cells, particularly during periods of nutrient limitation [51]. Overall, it was apparent that the mixed culture preferred to attach to the support. Of all the assisted carriers (supports) presented in this study, the cell count was highest in AC. This could be attributed to the fact that its surface area is higher than that of the others.

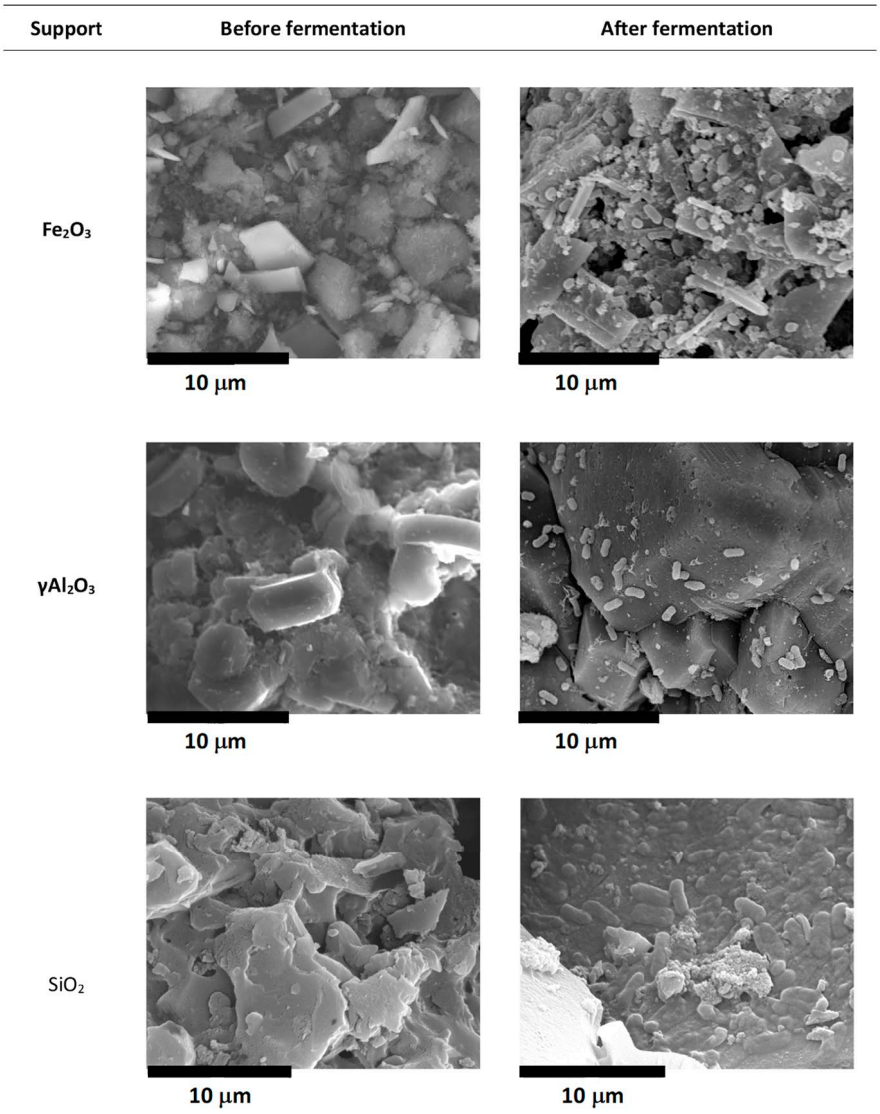

Figure 3. *Cont.*

Continued

Support	Before fermentation	After fermentation
Fe / SiO_2	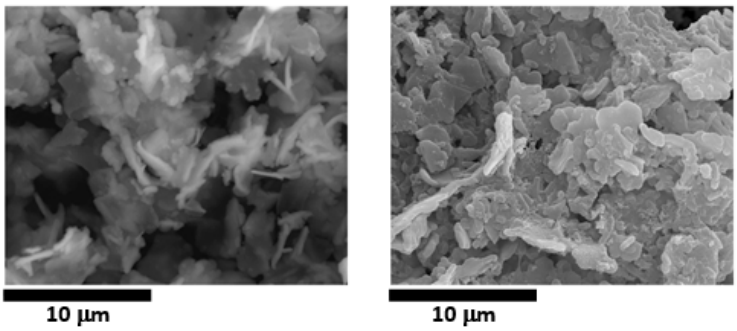	
AC	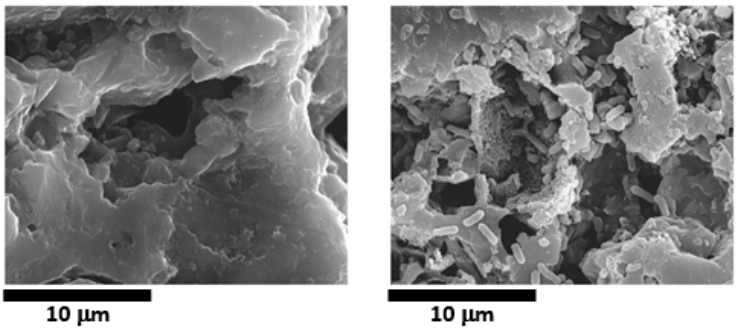	
Fe / AC	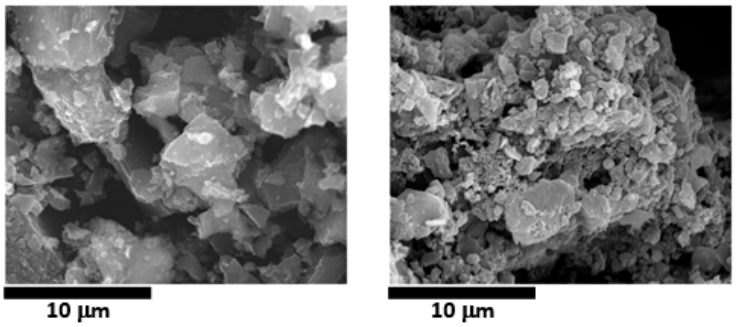	

Figure 3. SEM images of bare support and attached cells before and after dark fermentation.

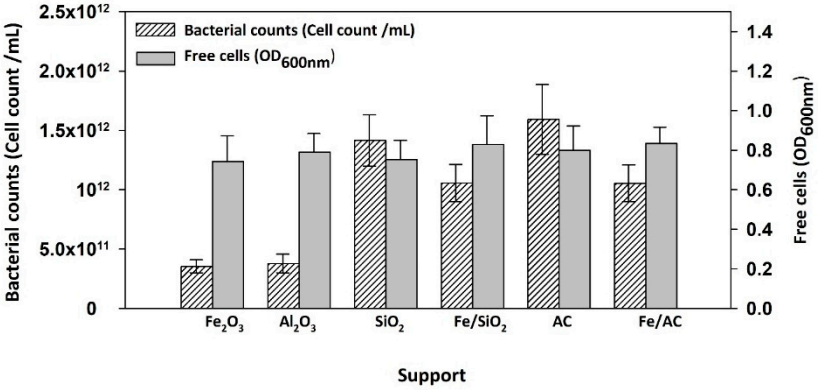

Figure 4. OD measurement for free cells and counts of attached cells on the support.

3.4. Effect of Supports and Iron on Glycerol Fermentation Products

Fermentative profile of glycerol metabolism by co-culture with and without support (the control) is shown in Figure 5a–g). The kinetics of the production of the fermentation product, H_2, in the carrier-supplemented cultures are also shown in Table 2. The use of assisted carriers in dark fermentation appeared to enhance the H_2 evolution, H_2 production rate, H_2 yield, and glycerol conversion efficiency in comparison to control (support-free) culture. Even though there were fewer cells attached in the Fe/AC and Fe/SiO_2 they produced significantly more H_2. This could be due to the contribution of iron to the metabolic pathways. Iron-sulfur species have an effect on protein functions primarily as electron carriers. Iron can also induce metabolic change and be involved in Fe–S and non-Fe–S proteins operating in hydrogenase [52]. The effect of each of the assisted carriers and the involvement of the iron species are discussed in more detail below.

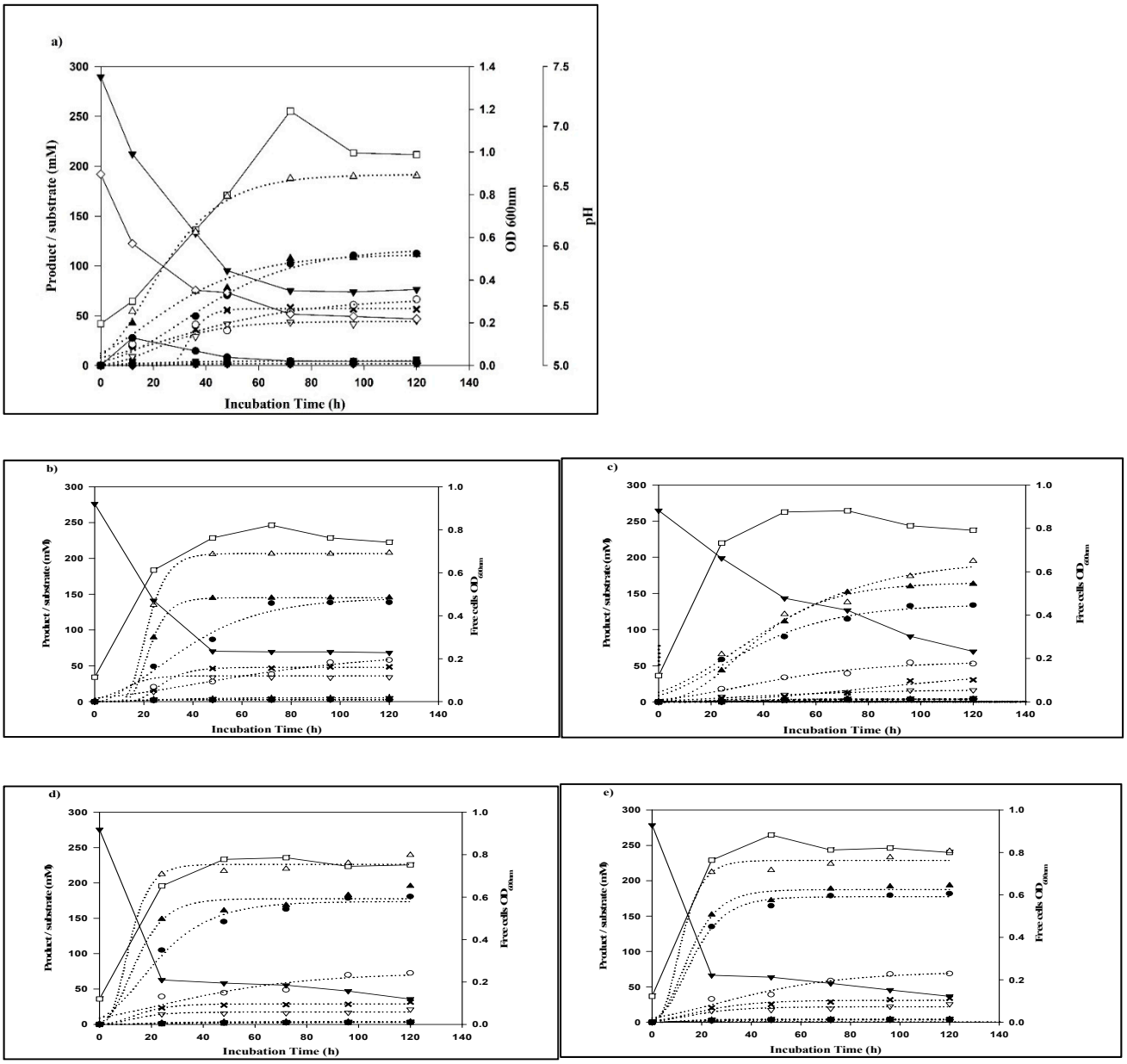

Figure 5. *Cont.*

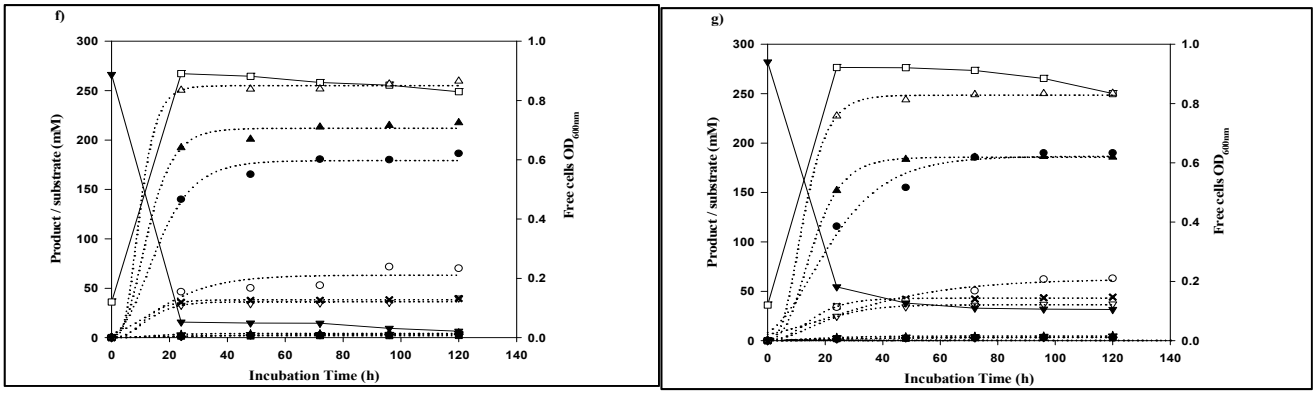

Figure 5. Glycerol fermentation profiles for a co-culture of *Enterobacter* spH1 and *Citrobacter freundii* H3 on support: (**a**) control without support (FC); (**b**) Fe_2O_3; (**c**) γ-Al_2O_3; (**d**) SiO_2; (**e**) Fe/SiO_2; (**f**) AC; (**g**) Fe/AC. Residual glycerol (▼), glycerol consumed (Δ), lactate (✕) acetate (■), 1,3-propanediol (∇), ethanol (▲), butyrate (♦), succinate(★),formate (●), H_2 (•), CO_2 (○), pH(◇) and $OD_{600\ nm}$ (□). The data was fitted using the modified Gompertz equation (Equations (1) and (2)) (dotted lines).

Furthermore, as an end metabolite, ethanol was observed to be higher in all assisted carriers (Figure 5b–f) compared to the FC (Figure 5a), meanwhile the other fermentation products, such as lactate, acetate, 1,3-propanodiol, butyrate, succinate and formate, are synthetized at lower concentrations (lower than 50 mM). Thus, this co-culture provides H_2 and ethanol as potential industrial products. This suggests that *Enterobacter* spH1 benefited from cell attachment in the co-culture. This is more consistent with our previous study [34], which found that *Enterobacter* spH1 was a higher producer of ethanol. A similar phenomenon has been noted in biofilms containing *Enterobacter* and *Citrobacter* and other mixed-species that occur naturally in water and food, where proportions of *Citrobacter* spp. are generally lower than *Enterobacter* spp [46,53,54].

3.5. Effect of Supports and Iron on H_2 Production and Metabolites

3.5.1. Effect of Supports on H_2 Production

According to the modified Gompertz equation (Equation (2)), the R_{max} (the kinetic characteristics of H_2 production at the highest production rate) was found to be slightly higher for Fe/AC (7.8 mmol/L/h) than AC (7.6 mmol/L/h), Fe/SiO_2 (7.3 mmol/L/h) and SiO_2 (4.4 mmol/L/h) (Table 2). All the assisted carriers (supports) presented higher H_2 production than the carrier-free cells (FC) for which H_2 production was 1.8 mmol/L/h.

In order to find an explanation for why the assisted support enhanced the H_2 mechanism, we monitored the morphology of the support surface before and after fermentation. Scanning electron microscopy (*SEM*) showed that cells attached to the surface of the AC support formed biofilms on the surface of the reactor. This suggests that the solid support may provide extra surface area for attached cell growth and possibly increase the mass diffusion transfer of the substrate and somehow increase H_2 production. Similarly, recent studies showed that biofilm formation on carriers (e.g., activated carbon and silica gel) plays a key role in enhancing biosurfactant production from *Bacillus subtilis* [55] and *Serratia marcescens* [56]. Additionally, the cell growth rate increased when solid carriers were added, especially when AC was used (Figure 4). This is consistent with previous reports which indicate that solid carriers such as silica gel and b-cyclodextrin could be effective growth stimulants [56,57]. The detailed mechanism of the carrier-induced promoting effects on dark fermentative H_2 production has yet to be clearly identified [33]. During the course of batch fermentation, the pH did not vary significantly compared with the FC (Table 2). Therefore, the two carriers (AC and SiO_2) were impregnated with iron and used for further investigation to determine their effect on H_2 production. The results indicate that the addition of iron can markedly enhance H_2 production in all categories (Tables 2 and 3).

Table 2. Maximum consumption and production.

Support	Initial Substrate	Maximal Consumption ($S_{max,i}$) and Production ($P_{max,i}$) *									Support	Glycerol Conversion	C-Balance	ξ-Reduction
		(mmol/L)										(%)	(%)	(%)
		S_{max}	$P_{max,EtOH}$	$P_{max,Lact}$	$P_{max,1,3PDO}$	$P_{max,Suc}$	$P_{max,Act}$	$P_{max,But}$	$P_{max,CO2}$	$P_{max,H2}$	Specific Area (m^2/g)			
FC	266.8	195.7	111.8	56.2	44.3	1.9	4.6	3.2	63.7	120.1		72	109.8	108.5
Fe_2O_3	276.2	213	143.1	49	35.1	5.2	3.2	2.4	67.2	156	205	78.4	107.7	107.6
Al_2O_3	264.7	196.6	165.3	28.2	17.1	3.3	3.8	3.8	55.9	135	253	72.3	104	107.2
SiO_2	275.6	226.4	182.9	29	17.4	3.9	3.1	3.1	73.3	174.8	685	83.3	100.6	102.7
Fe/SiO_2	278.8	228.8	182.6	38.1	21.8	4.2	3.9	3.3	71.9	183.5	440	84.2	104.1	106.2
AC	266.3	251	210.9	36.3	34.3	4.2	2	1.8	68.3	184.2	1195	92.4	107.8	112.9
Fe/AC	277.7	242.5	185.7	43.1	36.4	4.8	3.4	3.2	62.4	191.7	736	89.3	108	111.6

Support	Initial Substrate	Maximal Consumption ($R_{max,i}$) and Production Rate ($R_{max,\ i}$)									Support	Dry Cell Weight (DCW)	Final pH
		(mmol/L/h)										(g/L)	
		$R_{max,S}$	$R_{max,EtOH}$	$R_{max,Lact}$	$R_{max,1,3PDO}$	$R_{max,Suc}$	R_{maxAct}	$R_{max,But}$	$R_{max,CO2}$	$R_{max,H2}$			
FC	266.8	4.5	1.9	4.8	1.1	0.1	0.1	0.1	0.8	1.8	FC	1.25	5.39
Fe_2O_3	276.2	14.1	10.5	2.5	2.2	0.1	0.1	0.1	0.6	2.4	Fe_2O_3	1.58	5.61
Al_2O_3	264.7	2.4	3.2	0.4	0.2	0.1	0.1	0.3	0.7	2.1	Al_2O_3	1.65	5.81
SiO_2	275.6	15.9	8.6	1.3	0.8	0.1	0	0.1	0.8	4.4	SiO_2	1.88	5.82
Fe/SiO_2	278.8	15.2	9.1	0.8	0.6	0.2	0.1	0.1	0.9	7.3	Fe/SiO_2	2.05	5.72
AC	266.3	24.1	13.1	2.7	2.2	0.2	0.1	0.1	1.8	7.6	AC	2.22	5.87
Fe/AC	277.7	16.2	9.7	2.1	1.3	0.1	0.1	0.1	0.9	7.8	Fe/AC	2.19	5.66

Table 3. Maximum specific productivity and production.

Support		**Maximal Specific ($q_{max,i}$) and Production Rate (*qmax, i*)**								
		(mmol/gDCW × h)								
	Specific Area (m^2/g)	$q_{max,S}$	$q_{max,EtOH}$	$q_{max,Lact}$	$q_{max,1,3PDO}$	$q_{max,Suc}$	q_{maxAct}	q_{maxBut}	$q_{max,CO2}$	$q_{max,H2}$
FC		3.6	1.5	3.8	0.9	0.1	0.1	0	0.6	1.4
Fe_2O_3	205	8.9	6.6	1.6	1.4	0.1	0.1	0.1	0.4	1.5
Al_2O_3	253	1.4	2	0.2	0.1	0	0.1	0.2	0.4	1.3
SiO_2	685	8.4	4.5	0.7	0.4	0.1	0	0	0.4	2.4
Fe/SiO_2	440	7.4	4.2	0.4	0.3	0.1	0.1	0.1	0.4	3.6
AC	1195	10.8	5.9	1.2	1	0.1	0	0	0.8	3.4
Fe/AC	736	7.4	4.4	1	0.6	0.1	0	0	0.4	3.6
Support		**Molar Yields**								**Biomass Yield**
	Specific Area (m^2/g)	**(mol/mol)**								**$gDCW_{max}$/mol**
		Y_{EtoH}	Y_{Lact}	$Y_{1,3PDO}$	Y_{suc}	Y_{Act}	Y_{but}	Y_{CO2}	Y_{H2}	
FC		0.57	0.29	0.23	0.01	0.02	0.02	0.33	0.61	6.4
Fe_2O_3	205	0.67	0.23	0.17	0.02	0.01	0.01	0.32	0.73	7.4
Al_2O_3	253	0.84	0.14	0.09	0.02	0.02	0.02	0.28	0.69	8.4
SiO_2	685	0.81	0.13	0.08	0.02	0.01	0.01	0.32	0.77	8.3
Fe/SiO_2	440	0.8	0.15	0.1	0.02	0.02	0.01	0.31	0.8	9.0
AC	1195	0.84	0.14	0.14	0.02	0.01	0.01	0.27	0.74	8.8
Fe/AC	736	0.77	0.18	0.15	0.02	0.01	0.01	0.26	0.79	9.0

3.5.2. Effect of Iron on Glycerol Metabolites

The end liquid fermentative metabolites were of the same type, mainly 1,3-propanediol, ethanol and lactate with gaseous H_2 and CO_2. The effect of the support-assisted carrier in terms of surface area attachment and iron involvement can be seen in Tables 2 and 3 and Figure 6.

(i). Maximum H_2 production (mmol/L) and yield (mol H_2/mol glycerol consumed) increased in the following order: FC < γ-Al_2O_3 < Fe_2O_3 < SiO_2 < Fe/SiO_2 < AC < Fe/AC.

(ii). Maximum ethanol production (mmol/L) increased in the following order: FC < Fe_2O_3 < Al_2O_3 < SiO_2 < Fe/SiO_2 < Fe/AC < AC and the yield (mol EtOH/mol glycerol consumed) increased > > > > > FC < Fe_2O_3 < Fe/AC < Fe/SiO_2 < SiO_2 < AC < γ-Al_2O_3

(iii). Maximum 1,3-propanediol production (mmol/L) and yield (mol 1,3PDO/mol glycerol consumed) increased in the following order: γ-Al_2O_3 < SiO_2 < Fe/SiO_2 < AC < Fe_2O_3 < Fe/AC < FC.

(iv). Maximum lactate production (mmol/L) and yield (mol lactate/mol glycerol consumed) increased in the following order: γ-Al_2O_3 < SiO_2 < AC < Fe/SiO_2 < Fe/AC < Fe_2O_3 < FC.

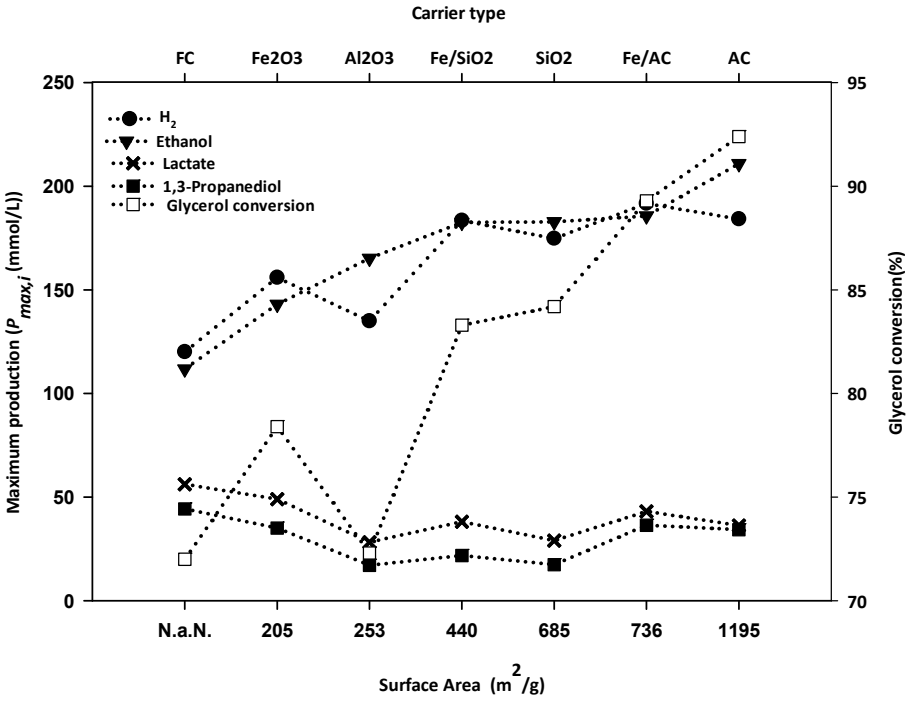

Figure 6. Effect of area and iron species on H_2, ethanol, 1,3-PDO and lactate production.

In previous work, we observed that the addition of 20–30 mg of Fe^{2+} (Fe_SO_4) also enhanced total hydrogen production [58]. Other studies have reported that iron-sulfur species have an effect on protein functions primarily as an electron carrier and it is involved in the oxidation of pyruvate to acetyl-CoA, CO_2 and H_2. Iron can also induce a metabolic change and may be involved in Fe–S and non-Fe–S proteins in hydrogenase.

3.6. Effect of Support on Glycerol Adsorption

In our reference experiments (only support), it was observed that H_2 or other metabolites were not produced without the culture. Due to adsorption, however, glycerol decreased over time. Figure 7 shows the capacity of each support to adsorb glycerol, calculated from the change in glycerol concentration in the solution according to Equation (1). As can be seen, the maximum amount of glycerol adsorbed is 150 mg/g of AC. Some reports on phenol adsorption tests also show a maximum capacity of 370 mg $_{ph}$/g_{AC} at 20 °C for the same active carbon support [44].

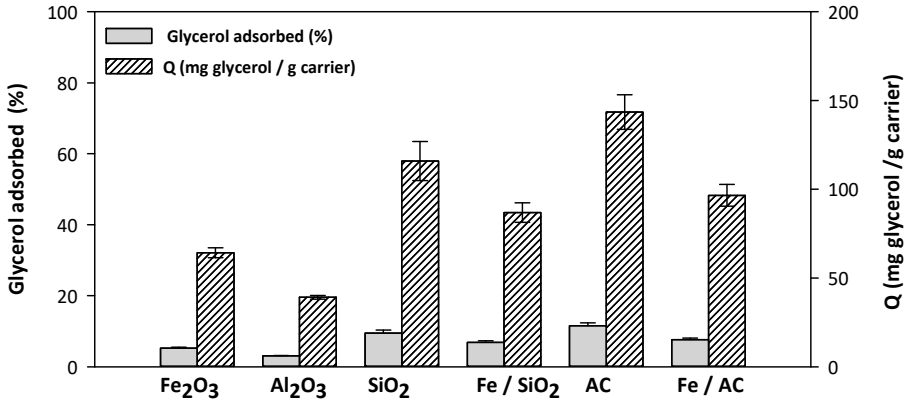

Figure 7. Effect of support on glycerol adsorption.

4. Conclusions

This study demonstrates that both support supplementation and iron played crucial roles in dark fermentation to produce H_2 from glycerol. Addition of iron species to the supports increased the H_2 production rate and yield when compared to the carrier-free culture.

Surface area attachment and iron involvement have been shown to have an effect on support carriers:

(i). For each of the supports, H_2 production (mmol/L) increased in the following order: FC (120) < γ-Al_2O_3(135) < Fe_2O_3(156) < SiO_2 (174) < Fe/SiO_2 (183)< AC (184) < Fe/AC (192).

(ii). Ethanol production (mmol/L) increased in the following order: FC(112) < Fe_2O_3 (143) < γ-Al_2O_3 (165) < SiO_2 (182) < Fe/SiO_2 (183) < Fe/AC (186) < AC (211).

(iii). 1,3-propanediol production (mmol/L) increased in the following order: γ-Al_2O_3 (16) < SiO_2 (17) < Fe/SiO_2 (22) < AC (34) < Fe_2O_3(35) < Fe/AC (36) < FC (45).

(iv). Lactate production (mmol/L) increased in the following order: γ-Al_2O_3(28) < SiO_2 (29) < AC (36) < Fe/SiO_2 (38) < Fe/AC (36) < Fe_2O_3(49) < FC (56).

The H_2 yield (mol H_2/mol glycerol consumed) was observed to be highest for Fe/AC.

Assisted carriers all follow different pathways, so the influence of the support on the enzymes participating in the metabolic activity needs to be studied in more detail.

The detailed mechanism of the support-induced effects on dark fermentative H_2 production has yet to be clearly identified and will be the focus of our future studies.

Author Contributions: Conceptualization, F.M. and M.C.; methodology, B.T.M., F.L., F.M. and M.C.; software, B.T.M.; validation, B.T.M., F.M. and M.C.; formal analysis, B.T.M., F.L., F.M. and M.C.; investigation, B.T.M., F.L., F.M. and M.C.; resources, F.M. and M.C.; data curation, B.T.M.; writing—original draft preparation, B.T.M.; writing—review and editing, F.M. and M.C.; visualization, B.T.M. and M.C.; supervision, F.M. and M.C.; project administration, F.M. and M.C.; funding acquisition, F.M. and M.C. All authors have read and agreed to the published version of the manuscript.

Funding: This study was funded by the Spanish Ministry of Science, Innovation and Universities, project RTI2018-098310-B-I00.

Conflicts of Interest: The authors declare no conflict of interest.

References

1. Das, D.; Veziroglu, T.N. Hydrogen production by biological processes: A survey of literature. *Int. J. Hydrogen Energy* **2001**, *26*, 13–28. [CrossRef]
2. Sung, S. *Biohydrogen Production from Renewable Organic Wastes, Finial Technical Report*; Iowa State University: Ames, IA, USA, 2004.
3. Zhang, Z.-P.; Show, K.-Y.; Tay, J.-H.; Liang, D.T.; Lee, D.-J. Enhanced continuous biohydrogen production by immobilized anaerobic microflora. *Energy Fuels* **2008**, *22*, 87–92. [CrossRef]
4. Lin, C.; Lay, C. A nutrient formulation for fermentative hydrogen production using anaerobic sewage sludge microflora. *Int. J. Hydrogen Energy* **2005**, *30*, 285–292. [CrossRef]

5. Levin, D.B.; Pitt, L.; Love, M. Biohydrogen production: Prospects and limitations to practical application. *Int. J. Hydrogen Energy* **2004**, *29*, 173–185. [CrossRef]
6. Carriquiry, M. U.S. biodiesel production: Recent developments and prospects, Iowa. *Agric. Rev.* **1997**, *13*, 8–9.
7. Yazdani, S.; Gonzalez, R. Anaerobic fermentation of glycerol: A path to economic viability for the biofuels industry. *Curr. Opin. Biotechnol.* **2007**, *18*, 213–219. [CrossRef] [PubMed]
8. Bickerstaff, G.F. *Immobilization of Enzyme and Cells*; Humana Press Inc.: Totowa, NJ, USA, 1997.
9. Gungormusler, M.; Tamayol, A.; Levin, D.B. Hydrogen production by immobilized cells of *Clostridium intestinale* strain URNW using alginate beads. *Appl. Biochem. Biotechnol.* **2021**, *193*, 1558–1573. [CrossRef]
10. Lee, K.-S.; Wu, J.F.; Lin, P.-J.; Chang, J.-S. Anaerobic hydrogen production with an efficient carrier-induced granular sludge bed bioreactor. *Biotechnol. Bioeng.* **2004**, *87*, 648–657. [CrossRef]
11. Boshagh, F.; Rostami, K.; Moazami, N. Immobilization of *Enterobacter aerogenes* on carbon fiber and activated carbon to study hydrogen production enhancement. *Biochem. Eng. J.* **2019**, *44*, 64–72. [CrossRef]
12. Chen, C.-Y.; Chang, J.-S. Enhancing phototropic hydrogen production by solid-carrier assisted fermentation and internal optical-fiber illumination. *Process. Biochem.* **2006**, *41*, 2041–2049. [CrossRef]
13. Lee, C.M.; Chen, P.C.; Wang, C.C.; Tung, Y.C. Photohydrogen production using purple nonsulfur bacteria with hydrogen fermentation reactor effluent. *Int. J. Hydrogen Energy* **2002**, *27*, 1309–1313. [CrossRef]
14. Wu, S.Y.; Hung, C.H.; Lin, C.N.; Chen, H.W.; Lee, A.S.; Chang, J.S. Fermentative hydrogen production and bacterial community structure in high-rate anaerobic bioreactors containing silicone-immobilized and self-flocculated sludge. *Biotechnol. Bioeng.* **2006**, *93*, 934–946. [CrossRef] [PubMed]
15. Lee, K.-S.; Lo, Y.-S.; Lo, Y.-C.; Lin, P.-J.; Chang, J.-S. Hydrogen fermentation with anaerobic sludge using activated-carbon supported packed-bed bioreactors. *Biotechnol. Lett.* **2003**, *25*, 133–138. [CrossRef] [PubMed]
16. Wu, S.-Y.; Lin, C.-N.; Lee, K.-S.; Lin, P.-J.; Chang, J.-S. Microbial hydrogen production with immobilized anaerobic cultures. *Biotechnol. Prog.* **2002**, *18*, 921–926. [CrossRef]
17. Mason, C.A.; Ward, G.; Abu-Salah, K.; Keren, O.; Dosoretz, C.G. Biodegradation of BTEX by bacteria on powdered activated carbon. *Bioprocess Eng.* **2000**, *23*, 333–336. [CrossRef]
18. Orshansky, F.; Narkis, N. Characteristics of organics removal by PACT simultaneous adsorption and biodegradation. *Water Res.* **1997**, *31*, 391–398. [CrossRef]
19. Fißler, J.; Kohring, G.W.; Giffhorn, F. Enhanced hydrogen production from aromatic acids by immobilized cells of *Rhodopseudomonas palustris*. *Appl. Microbiol. Biotechnol.* **1995**, *44*, 43–46.
20. Vincenzini, M.; Materassi, R.; Tredigi, M.R.; Florenzano, G. Hydrogen production by immobilized cells-light dependent dissimilation of organic substrates by *Rhodopseudomonas palustris*. *Int. J. Hydrogen Energy* **1982**, *7*, 231–236. [CrossRef]
21. Fang, H.H.P.; Liu, H.; Zhang, T. Phototrophic hydrogen production from acetate and butyrate in wastewater. *Int. J. Hydrogen Energy* **2005**, *30*, 785–793. [CrossRef]
22. Haag, R.; Roller, S. Polymeric Supports for the Immobilization of Catalysts. *Top. Curr. Chem.* **2004**, *242*, 1–42.
23. Juanita, M.; Guangyi, W. Metabolic pathway engineering for enhanced biohydrogen production. *Int. J. Hydrogen Energy* **2009**, *34*, 7404–7416.
24. Adams, M.W.W.; Mortenson, L.E.; Chen, J.S. Hydrogenase. *Biochim. Biophys. Acta* **1980**, *594*, 105–176. [CrossRef]
25. Vignais, P.M.; Billoud, B.; Meyer, J. Classification and phylogeny of hydrogenases. *FEMS Microbiol. Rev.* **2001**, *25*, 455–501. [CrossRef]
26. Shekhar, C.; Kai, T.; Garcia-Contreras, R. Evaluation of hydrogen metabolism by *Escherichia coli* strains possessing only a single hydrogenase in the genome. *Int. J. Hydrogen Energy* **2021**, *46*, 1728–1739. [CrossRef]
27. Valle, A.; Cantero, D.; Bolivar, J. Metabolic engineering for the optimization of hydrogen production in *Escherichia coli*: A review. *Biotechnol. Adv.* **2019**, *37*, 616–633. [CrossRef]
28. Nath, K.; Das, D. Improvement of fermentative hydrogen production: Various approaches. *Appl. Microbiol. Biotechnol.* **2004**, *65*, 520–529. [CrossRef] [PubMed]
29. Dabrock, B.; Bahl, H.; Gottschalk, G. Parameters affecting solvent production by *Clostridium pasteurianum*. *Appl. Environ. Microbiol.* **1992**, *58*, 1233–1239. [CrossRef]
30. Peguin, S.; Soucaille, P. Modulation of carbon and electron flow in Clostridium acetobutylicum by iron limitation and methyl viologen addition. *Appl. Environ. Microbiol.* **1995**, *61*, 403–405. [CrossRef]
31. Wu, H.; Wang, C.; Chen, P. Effects of pH and ferrous iron on the production of butanol and hydrogen by *Clostridium beijerinckii* IB4. *Int. J. Hydrogen Energy* **2017**, *42*, 6547–6555. [CrossRef]
32. Zhang, J.; Fan, C.; Zang, L. Improvement of hydrogen production from glucose by ferrous iron and biochar. *Biores. Technol.* **2017**, *245*, 98–105. [CrossRef]
33. Wu, K.-J.; Chang, J.-S. Batch and continuous fermentative production of hydrogen with anaerobic sludge entrapped in a composite polymeric matrix. *Process. Biochem.* **2007**, *4*, 2279–2284. [CrossRef]
34. Maru, B.T.; Constanti, M.; Stchigel, A.M.; Medina, F.; Sueiras, J.E. Biohydrogen production by dark fermentation of glycerol using *Enterobacter* and *Citrobacter* Sp. *Biotechnol. Progr.* **2013**, *29*, 31–38. [CrossRef]
35. Güell, E.J.; Maru, B.T.; Chimentão, R.J.; Gispert-Guirado, F.; Constantí, M.; Medina, F. Combined heterogeneous catalysis and dark fermentation systems for the conversion of cellulose into biohydrogen. *Biochem. Eng. J.* **2015**, *101*, 209–219. [CrossRef]

36. Gavilà, L.; Güell, E.J.; Maru, B.T.; Medina, F.; Constantí, M. Combining catalytical and biological processes to transform cellulose into high value-added products. In *Polymer Engineering*; Tylkowski, B., Wieszczycka, K., Jastrzab, R., Eds.; De Gruyter: Berlin, Germany; Boston, MA, USA, 2017; pp. 457–468.
37. Ito, T.; Nakashimada, Y.; Senba, K.; Matsui, T.; Nishio, N. Hydrogen and ethanol production from glycerol-containing wastes discharged after biodiesel manufacturing process. *J. Biosci. Bioeng.* **2005**, *100*, 260–265. [CrossRef]
38. Zazo, J.A.; Casas, J.A.; Mohedano, A.F.; Rodriguez, J.J. Catalytic wet peroxide oxidation of phenol with a Fe/active carbon catalyst. *Appl. Catal. B Environ.* **2006**, *65*, 261–268. [CrossRef]
39. Lindsay, D.; von Holy, A. Evaluation of dislodging methods for laboratory grown bacterial biofilms. *Food Microbiol.* **1997**, *14*, 383–390. [CrossRef]
40. Mu, Y.; Yu, H.; Wang, G. A kinetic approach to anaerobic hydrogen-producing process. *Water Res.* **2007**, *41*, 1152–1160. [CrossRef] [PubMed]
41. Seifert, K.; Waligorska, M.; Wojtowski, M.; Laniecki, M. Hydrogen generation from glycerol in batch fermentation process. *Int. J. Hydrogen Energy* **2009**, *34*, 3671–3678. [CrossRef]
42. Oh, Y.K.; Park, S.; Seol, E.H.; Kim, S.H.; Kim, M.S.; Hwang, J.W.; Ryu, D.D. Carbon and energy balances of glucose fermentation with hydrogen producing bacterium *Citrobacter amalonaticus* Y19. *J. Microbiol. Biotechnol.* **2008**, *18*, 532–538.
43. Converti, A.; Perego, P. Use of carbon and energy balances in the study of the anaerobic metabolism of Enterobacter aerogenes at variable starting glucose concentrations. *J. Appl. Microbiol. Biotechnol.* **2002**, *59*, 303–309.
44. Habtu, N.G. Catalytic Wet Air Oxidation of Phenol over Active Carbon in Fixed Bed Reactor: Steady State and Periodic Operation. Ph.D. Thesis, University of Rovira i Virgili, Tarragona, Spain, 2011.
45. Costerton, J.W.; Lewandowski, Z.; Caldwell, D.E.; Korber, D.R.; Lappin-Scott, H.M. Microbial biofilms. *Annu. Rev. Microbiol.* **1995**, *49*, 711–745. [CrossRef]
46. Thompson, L.J.; Gray, V.; Lindsay, D.; von Holy, A. Carbon: Nitrogen: Phosphorus ratios influence biofilm formation by Enterobacter cloacae and *Citrobacter freundii*. *J. Appl. Microbiol.* **2006**, *101*, 1364–5072. [CrossRef]
47. Donlan, R.M. Biofilms: Microbial life on surfaces. *Emerg. Infect. Dis.* **2002**, *8*, 881–890. [CrossRef] [PubMed]
48. Singh, P.; Patil, Y.; Rale, V. Biosurfactant production: Emerging trends and promising strategies. *J. Appl. Microbiol.* **2019**, *126*, 2–13. [CrossRef] [PubMed]
49. Choughuri, I.; Khanra, K.; Maity, P. Structure and biological properties of exopolisaccharide isolated from *Citrobacter freundii*. *Int. J. Biol. Macromol.* **2021**, *168*, 537–549. [CrossRef] [PubMed]
50. Cowan, M.M.; Warren, T.M.; Fletcher, M. Mixed species colonization of solid surfaces in laboratory biofilms. *Biofouling* **1991**, *3*, 23–34. [CrossRef]
51. Lindsay, D.; von Holy, A. What food safety professionals should know about bacterial biofilms. *Br. Food J.* **2006**, *108*, 27–37. [CrossRef]
52. Lee, Y.; Miyahara, J.; Noike, T. Effect of iron concentration on hydrogen fermentation. *Bioresour. Technol.* **2001**, *80*, 227–231. [CrossRef]
53. Gauthier, F.; Archibald, F. The ecology of "fecal indicator" bacteria commonly found in pulp and paper mill water systems. *Water Res.* **2001**, *35*, 2207–2218. [CrossRef]
54. Sharma, M.; Anand, S.K. Biofilms evaluation as an essential component of HACCP for food/dairy processing industry—A case. *Food Control* **2002**, *13*, 469–477. [CrossRef]
55. Yeh, M.-S.; Wei, Y.-H.; Chang, J.-S. Enhanced production of surfactin from *Bacillus subtilis* by addition of solid carriers. *Biotechnol. Progr.* **2005**, *21*, 1329–1334. [CrossRef] [PubMed]
56. Yamashita, M.; Nakagawa, Y.; Li, H.; Matsuyama, T. Silica gel-dependent production of *prodigiosin* and *serrawettin*s by *Serratia marcescens* in a liquid culture. *Microb. Environ.* **2001**, *16*, 250–254. [CrossRef]
57. Imaizumi, A.; Suzuki, Y.; Ono, S.; Sato, H. Heptakis (2,6-O-dimethyl) bcyclodextrin: A novel growth stimulant for *Bordetella pertussis* phase I. *J. Clin. Microbiol.* **1983**, *17*, 781. [CrossRef] [PubMed]
58. Maru, B.T.; Medina, F.; Sueiras, J.E.; Stchigel, A.M. Biohydrogen production from different biodegradable substrates through dark fermentation. *New Biotechnol.* **2009**, *25*, 216–217. [CrossRef]